Catalysis Communications 174 (2023) 106578

Contents lists available at ScienceDirect

Catalysis Communications

journal homepage: www.elsevier.com/locate/catcom

Fe-Mn/ZrO_2 catalysts: Sulfate-based-advanced oxidation process for the degradation of olive oil industry model pollutants

Camila M. Loffredo, Mariana Dennehy, Mariana Alvarez *

INQUISUR/ Departamento de Química, Universidad Nacional del Sur, Av. Alem 1253, 8000 Bahía Blanca, Argentina

ARTICLE INFO

Keywords:
ZrO_2
Organic pollutants
Advanced oxidation processes
Sulfate radicals
iron and manganese catalysts

ABSTRACT

Fe, Mn and a bimetallic Fe—Mn catalysts supported on ZrO_2 were synthesized and tested for the activation of persulfate (PS) and peroxymonosulfate (PMS) in the degradation reaction of three different organic compounds: cinnamic acid (CA), benzoic acid (BA), and catechol (C). The catalysts were prepared and tested in order to evaluate the effect of the metal and the metal combination on the generation of reactive oxygen species (ROS). The characterization of the catalysts was carried out by X-ray diffraction (XRD), X-ray photoelectron spectroscopy (XPS), and atomic absorption spectroscopy (AAS).

The best degradation results were obtained when PMS was activated with the bimetallic Fe-Mn/ZrO_2 catalyst in the CA degradation. Moreover, the Fe-Mn/ZrO_2 catalyst reusability was tested for up to three consecutive cycles of reaction, with mineralization levels >90%.

A synergistic effect between the Fe and Mn metal species, which increases the catalyst activity if compared to the monometallic catalysts, is postulated. Both sulfate and hydroxyl radicals were generated in the PMS activation process. The activation mechanisms of the oxidants were proposed.

1. Introduction

When certain phenolic and aromatic compounds are released into aquatic or soil environments, they can generate adverse effects if their concentrations exceed certain levels [1,2]. Many of these organic pollutants are not biodegradable, thus they can accumulate in the organism and generate potential damage due to their toxicity (induction of carcinogenesis, teratogenesis, and mutagenesis, among others) [3]. In order to avoid these unwanted effects, the compounds have to be degraded or modified. Some agro-industries produce large quantities of wastewaters containing phenolic pollutants. As an example, olive oil production involves producing considerable amounts of liquid effluent, which is referred to as olive mill wastewater (OMW). Different compounds can be found in OMW, such as hydroxytyrosol and catechins (ranging from 100 to 1400 mg L^{-1} [4–6]) derived from catechol (1,2-dihydroxybenzene, C) and cinnamic acid (acid(E)-3-phenyl-2-propenoic, CA) which concentration in OMW can reach up to 106 mg L [7]. Furthermore, the presence of benzoic acid (BA) derived compounds, such as p-hydroxybenzoic acid, gallic acid, vanillic acid, and protocatechuic acid were reported in concentrations in the range of 20 ppm in different OMW samples [8].

While some articles report the application of biological degradation [9] to eliminate these pollutants, advanced oxidation processes (AOP) were also employed for this purpose [10]. AOPs are based on the oxidation of organic chemicals by in situ generated reactive oxygen species (ROS) like hydroxyl (•OH) or sulfate ($SO_4^{\bullet-}$) free radicals. Sulfate radicals can be produced by the catalytic activation of peroxymonosulfate (PMS) or persulfate (PS) anions [11,12]. For that purpose, the use of green and low-cost catalysts is highly desirable. Iron and manganese-based catalysts have been extensively studied due to their low cost and because they are non-toxic metals. However, bare Fe_3O_4 and Fe_2O_3 showed, in general, low catalytic performances [13]. Moreover, a synergistic effect between Fe and Mn has been reported [14], turning these bimetallic catalysts to be active towards the activation of PMS [15–17] and PS [18–20]. Zirconia (Z)-based oxides are very interesting materials to be applied as metal catalyst supports because of their unique redox and acid-base properties [21,22]. Metal-modified ZrO_2 as well as ternary mixed oxide containing ZrO_2 have been reported for the photodegradation of organic pollutants, such as naproxen and different dyes [23–25]. Moreover, Fe_2O_3-ZrO_2 catalyst has been applied for phenol degradation in a Fenton-like reaction [26]. Recently, Sakthisharmila et al. reported the use of Mn and Fe doped ZrO_2

* Corresponding author.
E-mail addresses: camila.loffredo@uns.edu.ar (C.M. Loffredo), mdennehy@uns.edu.ar (M. Dennehy), alvarezm@criba.edu.ar (M. Alvarez).

https://doi.org/10.1016/j.catcom.2022.106578
Received 20 October 2022; Received in revised form 24 November 2022; Accepted 1 December 2022
Available online 5 December 2022

composites as photocatalysis employed in the degradation of textile dyes [27]. However, to our knowledge, there are no reports of the use of Fe-Mn/ZrO_2 catalysts for sulfate radical-based oxidation degradations of phenolic compounds. For these reasons, we decided to explore the activity of different Fe and/or Mn catalysts, supported on ZrO_2 (Z) in the degradation of three model organic compounds that could be present in OMWs: C, CA and BA.

2. Experimental

2.1. Synthesis of the catalysts

Mono- and bimetallic Fe—Mn catalysts supported on Z were prepared, with a total nominal metal content up to 4%wt. The obtained materials were named Fe_xMn_y, being x and y the nominal content of each metal in the catalyst. The employed synthesis for the preparation of the catalysts was previously reported by Garcia et al [28] In brief, NH_4OH (28% in NH_3) was added to a 0.4 M zirconium oxychloride solution, at room temperature, until pH 10. Zirconium hydroxide $Zr(OH)_4$ was then obtained as a pale yellow precipitate. Incipient wetness impregnation was employed for the Fe and/or Mn deposition. For that purpose, $Fe(NO_3)_3$ and $Mn(NO_3)_2$ aqueous solutions of the desired concentration were added to the zirconium hydroxide. The liquid to solid ratio was kept as 0.4 mL/g [29]. Finally, the solids were dried in air and kept at 383 K for 24 h. Then, they were calcined at 873 K in air for 4 h.

2.2. Catalysts characterization

An X'Pert Pro PANalytical Diffractometer, with Cu Kα radiation (40 mA, 45 kV) (2θ-range of 10–80°) and PIXcel3D detector (step size of 0.01313°) was used to register X-ray diffraction (XRD) patterns of the catalysts.

The metal content of the different samples was measured by atomic absorption spectroscopy (AAS) (Avanta GBC AA-932 spectrometer). The solutions were prepared dissolving 30 mg of each catalyst with 1 mL of 40% HF and 1 mL of concentrated HCl at 70 °C.

The oxidation state of the surface metal species (before and after the reaction) was determined by X-ray photoelectron spectroscopy (XPS) (PHI 548 spectrometer) with a double pass cylindrical mirror analyzer, using non-monochromatic Al Kα radiation (1486.6 eV). High-resolution spectra of C 1 s, O 1 s, Mn 2p, and Fe 2p were recorded, and the binding energies were recalibrated based on the C 1 s line at 284.8 eV. Spectra analysis and peak deconvolution was performed with OriginPro 9.0 software, using a polynomial spline baseline and a Gaussian function.

2.3. Catalytic activity

PMS was used as part of the triple salt commercially known as Oxone® ($KHSO_5$•½$KHSO_4$•½K_2SO_4), while PS was used in the form of its potassium salt ($K_2S_2O_8$). All the reactions were carried out in a glass batch reactor, containing 75 mL of a solution of 20 mg L^{-1} of CA, 50 mg L^{-1} of C, or 30 mg L^{-1} of C at 30 °C. The reactions were carried out without adjustment of pH. The solid oxidant (0.285 g of PMS or PS) and the catalyst (0.100 g) were added into the initial pollutant solution, under constant mechanical stirring. Suspension aliquots (3 mL) were withdrawn at predetermined intervals and filtered immediately through a Micropore membrane (pore size 0.45 μm). The UV–Visible spectra were collected (λ = 200–600 nm) in UV–Vis Cecil 2021 or UV–Vis Agilent Cary 60 spectrometers. The reactions were followed up to 240–270 min. The decrease in the main absorption bands of the contaminants, characteristics of the π → π * transition in aromatic compounds (λ_{max} BA = 228.0 nm at pH = 4.3; λ_{max} C = 275.5 nm at pH = 5; λ_{max} CA = 279.0 nm at pH = 4.7) was followed to evaluate the progress of the degradation reaction.

Control experiences were carried out to evaluate the degradation of the contaminants with the oxidizing agent in the absence of catalyst. In addition, the possible adsorption of the pollutants onto the catalyst surface was also analyzed. Moreover, the activity of the Z support without metal loading was evaluated in the degradation reactions.

The consumption of the oxidant during the reaction was followed and determined using spectrophotometric methods [30,31], mainly based on the reactions of the remnant PS and PMS anions with I^- (Eq. 1 and Eq. 2). The colored complex that appears after the reaction has a strong absorption band with a maximum at 395 nm (reaction with PMS) and 352 nm (reaction with PS).

$$HSO^-_{5\ (ac)} + 3\ I^-_{(ac)} \rightarrow SO^{2-}_{4\ (ac)} + I^-_{3\ (ac)} \quad (1)$$

$$S2O8^{2-}_{(ac)} + 3\ I^-_{(ac)} \rightarrow 2\ SO^{2-}_{4\ (ac)} + I^-_{3\ (ac)} \quad (2)$$

The Total Organic Carbon (TOC) remaining in the solutions was measured using a TOC-LCPH/NPC (Shimadzu) in order to evaluate de degree of mineralization of the phenolic contaminants. It was calculated according to the following relationship:

$$\%\text{of mineralization} = \left(\frac{TOC_0 - TOC_t}{TOC_0}\right) \times 100$$

where TOC_0 (mg L^{-1}) is the total organic carbon in the initial solution and TOC_t (mg L^{-1}) is the TOC concentration at the reaction time t.

The pH of the initial solutions and the residual liquids after reaction was measured with a pH-meter Orion 250Aplus equipped with a pH electrode.

The stability of the catalysts was tested by AAS through the measurement of the leached metals in the remaining solution after 4 h of reaction.

Quenching experiments were performed in order to determine the main ROS responsible for the degradation of pollutants. For that purpose, the reactions were repeated as it was described before with the addition of either tertbutyl alcohol (TBA) or ethanol (EtOH) [32]. An adequate amount of each alcohol in the respective reactions was added into the reactor before the addition of the catalyst and the oxidant. The alcohol: oxidant molar ratio was 150:1.

2.4. Reusability tests

The reusability of the catalysts in successive cycles was studied in the CA and C degradation reactions, under the same reaction conditions, with PMS as oxidizer. For that, at the end of the reaction the recovered solid was immediately washed with double distilled water, and dried at 30–40 °C.

3. Results and discussion

3.1. Catalysts characterization

All the catalysts presented similar diffraction patterns (Fig. 1). Peaks observed at 2θ values of 30.2° (101), 35° (110), 50.2° (112), and 60.2° (211), revealed that the ZrO_2 presented a tetragonal phase crystal structure (JCPDS file number 42–1164) with some low intensity peaks at 28.3° (−111), 63.1° (131) and 74.7° (−401) that would indicate traces of the ZrO_2 monoclinic phase (JCPDS file number 37–1484) [33,34]. The XRD patterns do not show peaks attributable to Fe or Mn oxides. The absence of those signals could be an indication of a high degree of dispersion of the metal species on the support.

The metallic content of the catalysts is presented in Table 1. As can be seen, the presence of Mn would promote the dispersion of Fe on the support surface, in the bimetallic material.

XPS analysis was carried out to determine the detailed valence states of Mn and Fe in the prepared materials. The XPS spectra of the catalysts of the Fe 2p and Mn 2p regions are shown in Fig. 2. According to the Gaussian fitting method, the Fe 2p spectra for Fe_2Mn_0 and Fe_2Mn_2

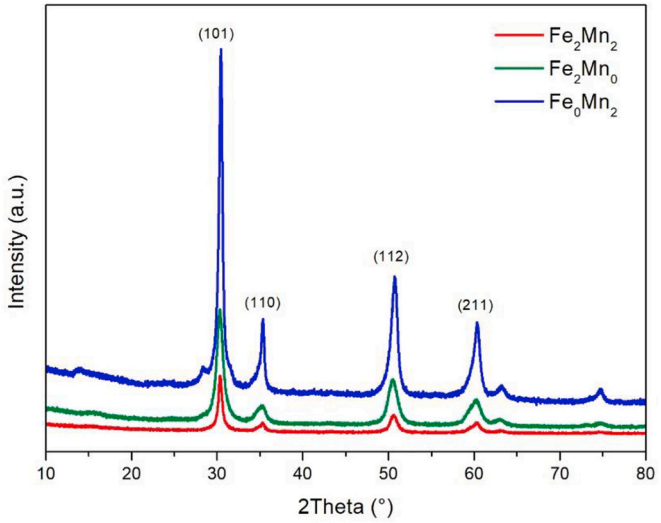

Fig. 1. XRD patterns of the prepared catalysts.

Table 1
Measured metallic content of the catalysts.

Catalyst	Metallic content (w%)	
	Fe	**Mn**
Fe_2Mn_0	1.08	–
Fe_2Mn_2	1.71	1.06
Fe_0Mn_2	–	0.95

showed signals at ca. 710 and 713 eV, indicating the existence of Fe(II) and Fe(III) species [17,35,36]. The Mn 2p3/2 spectrum of monometallic Fe_0Mn_2, on the other hand, showed two deconvoluted peaks at 642.1 and 646.9 eV, which were assigned to Mn(III) and Mn(II) oxidation states, respectively [37]. These results would indicate that the oxidation states of Mn and Fe in these samples coexisted as mixed phases.

However, the Mn 2p spectrum of bimetallic Fe_2Mn_2 showed significant differences: two peaks with binding energies of 640.3 eV and 645.2 eV, corresponding to Mn(II) and a "shakeup" peak, respectively. This last peak is originated from the charge transfer from the outer electronic layer towards an unoccupied orbital of higher energy during the photoelectronic process [38]. Therefore, it would seem that the simultaneous presence of Mn(II) and Fe(III) in the impregnation of the ZrO_2 support would retard the oxidation of Mn(II) to species with higher oxidation state.

3.2. Catalytic activity

3.2.1. Control experiences

Preliminary experiments were carried out to evaluate the individual effect of the catalyst with the highest metal loading (Fe_2Mn_2) and the two oxidants (PS and PMS) on the degradation of the three pollutants, including adsorption on the catalyst surface and non-catalytic chemical oxidation.

The control experiments employing only oxidants without catalyst showed that BA, C, and CA are only partially oxidized with PS or PMS, since bands of different intensities are still observed after 180 min of reaction for the three pollutants. These results indicate that none of the three pollutants can be efficiently degraded using only the oxidants in the studied conditions (Fig. 1, a-c, Suppl. Material).

In the presence of Fe_2Mn_2 material and without oxidant addition, around 37% of CA elimination was achieved after 180 min of reaction (Fig. 2, Suppl. Material). Based on the spectral profile, it could be inferred that the removal occurs by adsorption of CA on the catalyst surface and no degradation took place.

The CA degradation profiles obtained using PMS and employing PMS with the Z support (no metal) were similar, corroborating the inertia of the support to effectively activate the oxidant (Fig. 3, Suppl. Material).

3.2.2. Degradation experiences using PMS as an oxidizer

The spectra profiles at different times of reaction of BA degradation with PMS are showed in Fig. 3. When Fe_2Mn_2 catalyst was employed (Fig. 3-a), an increase in the intensity of the characteristic band at 228 nm is observed as the reaction progresses, slowing down the reaction rate as time goes by. Similar results were obtained using Fe_2Mn_0 and Fe_0Mn_2 samples in the same conditions (Fig. 3 b-c). It is noteworthy the resistance of BA to oxidative degradation under the experimental conditions of this work.

Regarding the degradation reactions of C employing the three different catalysts the intensity of the band at 275 nm increases in the earlier times of reaction and then decreases. But completely band-free spectra are not achieved at the studied reaction time in none of these three cases (Fig. 4).

A significant decrease in the 279 nm band is observed from the beginning when Fe_2Mn_2 is used as catalyst in the CA degradation (Fig. 5 a). This trend is accentuated as the reaction time increases, and almost a complete disappearance of the band is observed after 240 min. This behavior is also observed when the monometallic catalysts are employed (Fig. 5 b-c).

The different behavior towards the degradation of the studied pollutants, under the same experimental conditions could be explained based on the report of Oh et al. [39] Considering the electrophilicity of the $SO_4^{\bullet-}$ radical, it is expected to react with electron-donor groups such as amino ($-NH_2$), hydroxyl (–OH), alkoxy (–OR), π electrons of aromatic molecules and other organic compounds containing unsaturated bonds. With electron withdrawing substituent groups such as nitro ($-NO_2$) and carbonyl (C=O), the radical reaction is slower. For this reason, C and CA appear to be more prone to the oxidative degradation than BA. Considering the reaction of the three contaminants with both oxidants, employing the three catalysts, CA showed the greatest rate of degradation, based on the reduction of the intensity of the main aromatic absorption band.

For comparative purposes, the spectra of the residual liquids of the degradation of CA reaction, with the three catalysts, are presented in Fig. 6, after 240 min of reaction. From these results, Fe_2Mn_2 appears to be the catalyst with the best performance through CA degradation using PMS as oxidant. For this reason, this catalyst is employed to evaluate its activity in the PS activation in subsequent experiments. (See Fig. 7.)

3.2.3. Degradation experiences using PS as an oxidizer and Fe_2Mn_2 as catalyst

In the case of BA with PS and Fe_2Mn_2 (Fig. 4, Suppl. Material), an increase in the characteristic bands is observed as the reaction proceeds, showing a similar behavior than the reported activity for PMS-mediated degradation (Fig. 4).

The degradation spectra of C are observed in Fig. 8. The 275 nm band decreased as the reaction proceeds, reaching a constant profile after 240 min. During the reaction, a band around 385 nm of variable intensity appears together with the development of brownish color in the reaction liquid. After a short period, it disappears. These observations are consistent with those reported by Mijangos et al. [40] and Lin et al. [41] on phenol oxidation by AOP-based reactions. The color development could be attributed to a mixture of intermediate compounds including p-benzoquinone (yellow), o-benzoquinone (red), and hydroquinone (colorless). This effect may also have occurred when using PMS, but it was not clearly observed because of its faster kinetics under these conditions (Fig. 3).

For CA (Fig. 8) degradation reaction, the band around 279 nm diminishes but is still present after 240 min of reaction, indicating that in these conditions the degradation of CA is less efficient than the

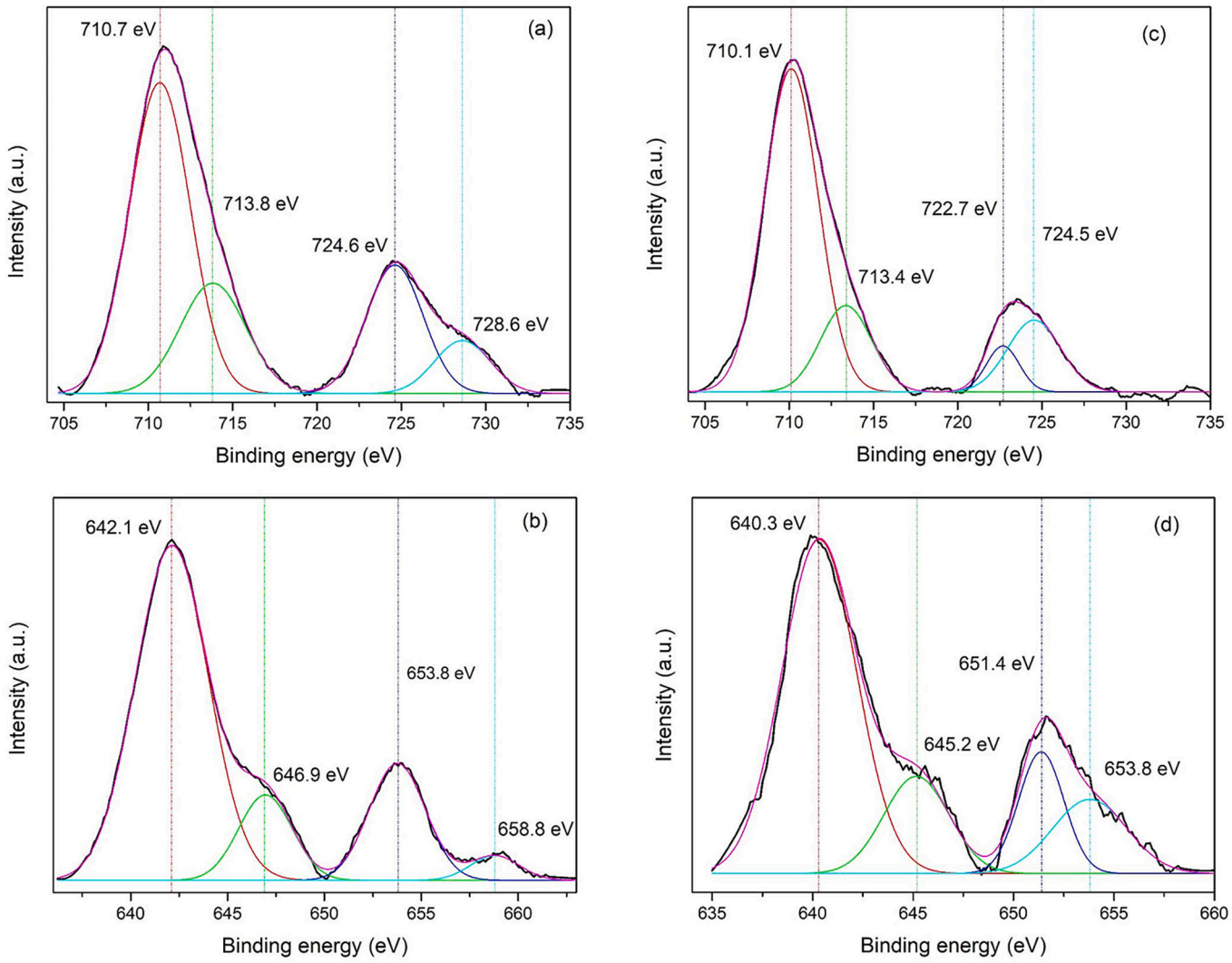

Fig. 2. XPS spectra of the three catalysts. a) Fe 2p in Fe_2Mn_0, b) Mn 2p in Fe_0Mn_2, c) Fe 2p in Fe_2Mn_2 and c) Mn 2p in Fe_2Mn_2.

degradation with PMS.

Based on the spectral profiles, it can be inferred that a similar low degradation rate of BA was achieved using either PS or PMS at comparable reaction times. Moreover, both oxidants are highly active towards C degradation. However, the CA/PMS combination showed the best results in terms of degradation, regardless of the tested catalyst.

The difference between the results working with PS compared to PMS could be due to the structural differences between both anions; while the PS activation proceeds through a homolytic cleavage of a peroxide bond in its symmetric structure, the asymmetry of the PMS allows greater easiness in the breaking of the bond, therefore it would present a greater reactivity towards the formation of $SO_4^{\bullet-}$, with a consequent increase the efficiency in the degradation [42].

3.2.4. Radical inhibitors

In order to identify the main radical contributions for the degradation of CA, the reaction kinetics were repeated in the presence of radical trapping agents (EtOH and TBOH) employing the Fe_2Mn_2 catalyst (Fig. 5 Suppl. Material). It can be seen that the degradation of CA was inhibited by the presence of alcohols in both cases, although when TBOH, a selective $OH^{\bullet}$ radical scavenger, was added the decrease of the 279 nm band intensity was more marked. On the other hand, when the reaction was carried out in the presence of EtOH, that has relatively comparable reaction kinetics with $OH^{\bullet}$ and $SO_4^{\bullet-}$ radicals, the CA UV–Vis profile does not show significant changes after 3 h of reaction.

These facts would indicate not only that the reaction occurs by radical pathways, but also that both $SO_4^{\bullet-}$ and $OH^{\bullet}$ radicals (that may be generated from $SO_4^{\bullet-}$) would be the main responsible species in the transformation of the substrate.

3.2.5. Leaching of metal species

Leaching of metal ions is a major problem for heterogeneous catalysts in liquid phase reaction. However, manganese oxides and iron oxides are quite environmentally friendly catalysts considering the lower potential toxicity of the leaching ions. For that reason, the leaching of Fe and Mn ions into the pollutant solutions during the reaction was evaluated. The Fe leaching from Fe_2Mn_0 catalyst was ca. 7.0–7.8% and only 1.4–1.7% was measured from Fe_2Mn_2. On the other hand, ca. 22.4–27.0% of Mn leaching for both the monometallic and bimetallic catalysts was achieved.

3.3. Mineralization and reusability tests

The evaluation of the reusability of catalysts is essential because the long-term stability is a significant factor for effective catalysts and is crucial for its practical application. Three sequential experiments were carried out to evaluate the reusability of the catalysts. TOC was measured after each run to determine the catalytic efficiency in each

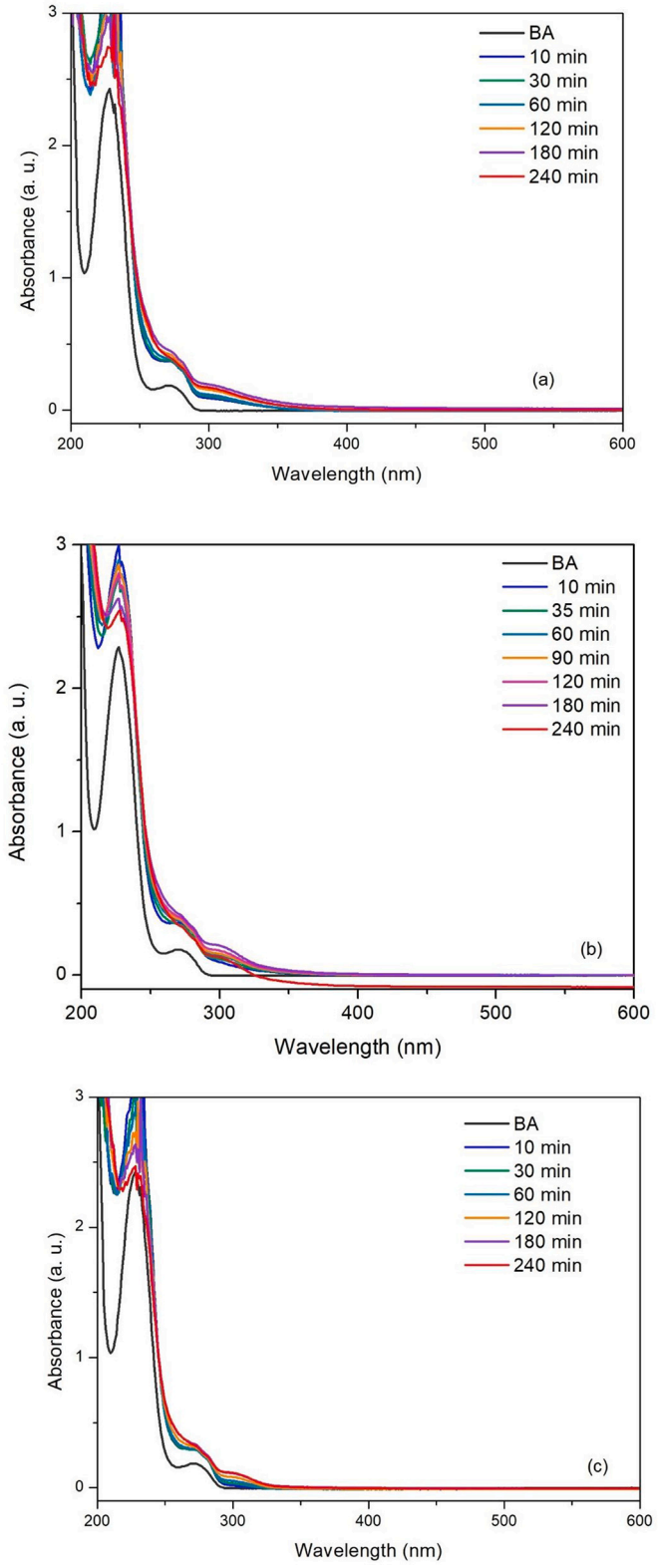

Fig. 3. UV–Vis spectrum: BA degradation with PMS and different catalysts. a) Fe_2Mn_0 b) Fe_2Mn_2 C) Fe_0Mn_2.

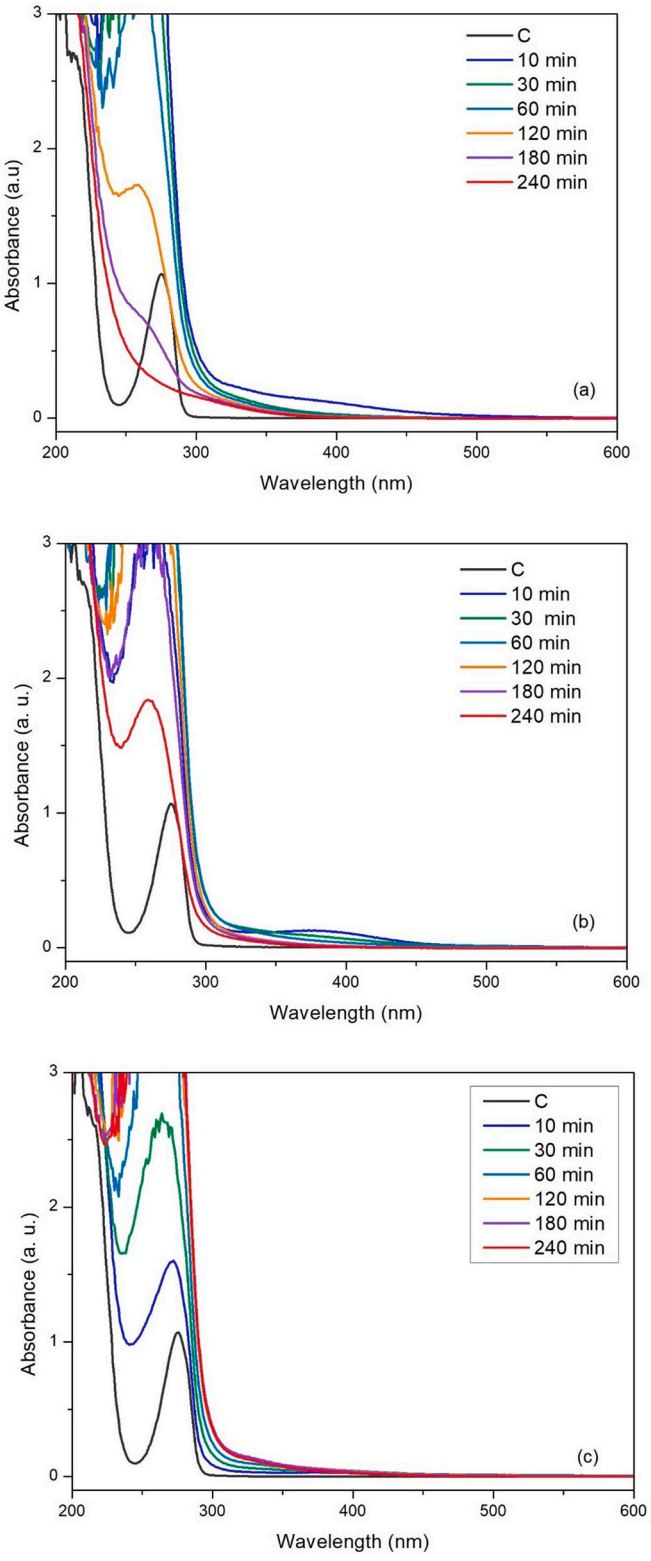

Fig. 4. UV–Vis spectrum: C degradation with PMS and different catalysts. a) Fe_2Mn_0 b) Fe_2Mn_2 C) Fe_0Mn_2.

cycle with respect to the mineralization of organic contaminants. Fig. 9 shows the % mineralization for each reusability test for CA degradation using PMS, and mono- and bimetallic catalysts.

As can be seen, when Fe_2Mn_2 is used as catalyst, TOC removal reached >90% in the three cycles of use. However, when monometallic catalysts were tested, the % mineralization decreased after each reutilization cycle. This trend is more pronounced in the case of Fe catalyst (from 70% in the first use to 7% in the third use) than in the Mn catalyst (from 85% to 65%).

The best efficiency found for the bimetallic material could be attributed to a synergistic effect between Fe and Mn species, which

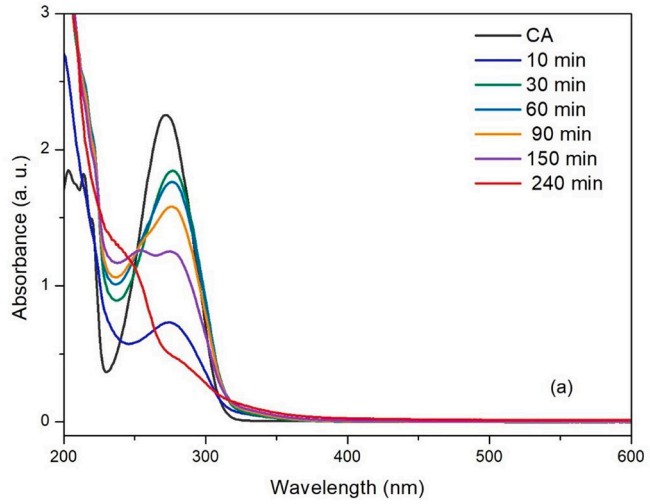

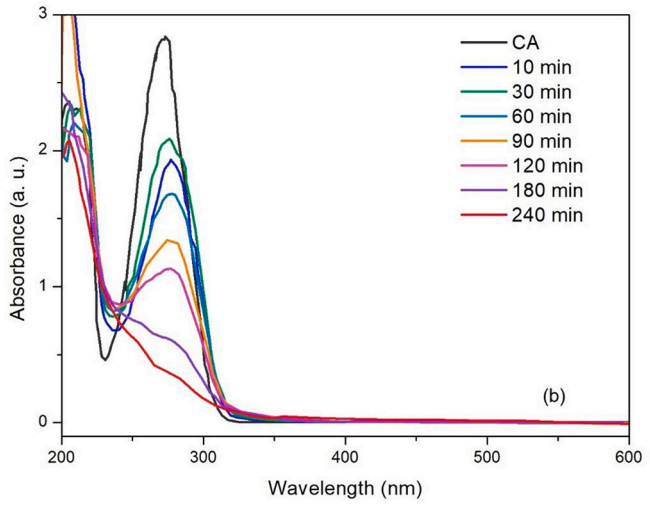

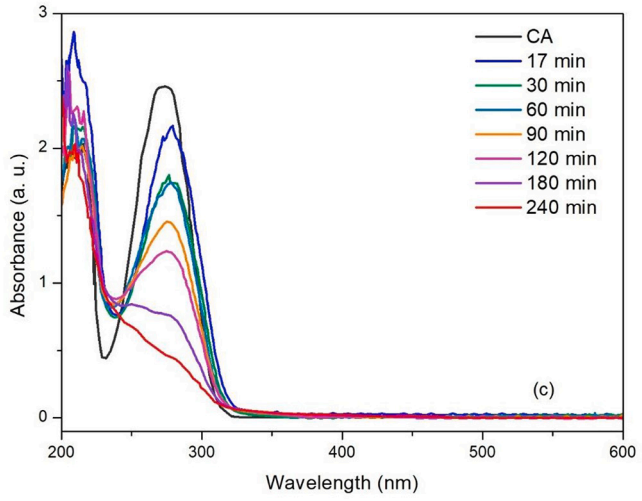

Fig. 5. UV–Vis spectrum: CA degradation with PMS and different catalysts. a) Fe_2Mn_0 b) Fe_2Mn_2 C) Fe_0Mn_2.

would improve the catalytic activity even after several cycles of use, with respect to monometallic catalysts.

To further understand this behavior and possible synergistic effects of Fe and Mn in the oxidant activation mechanism, XPS was used to evaluate the chemical composition of active species for the fresh (Fig. 2-

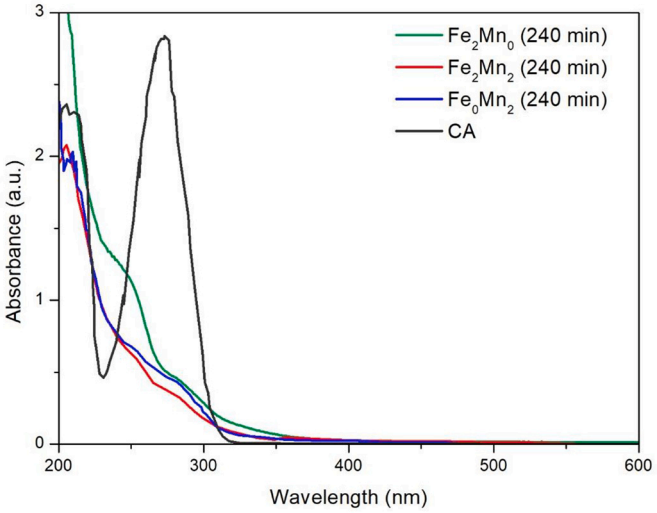

Fig. 6. UV–Vis spectrum: CA degradation with PMS and Fe—Mn catalysts at 240 min of reaction.

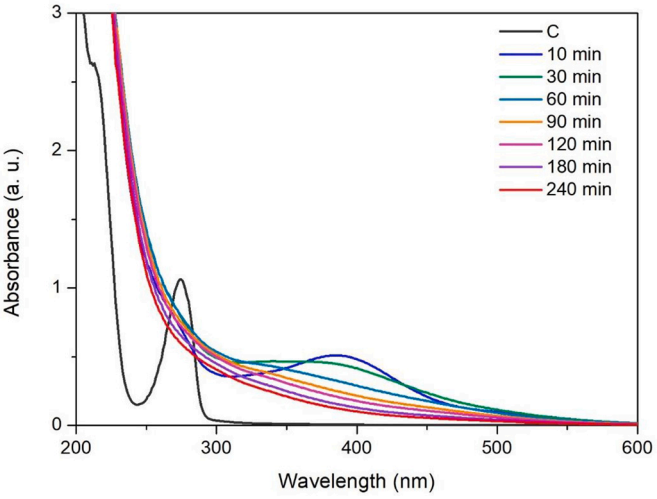

Fig. 7. UV–Vis spectrum: C degradation with PS and Fe_2Mn_2.

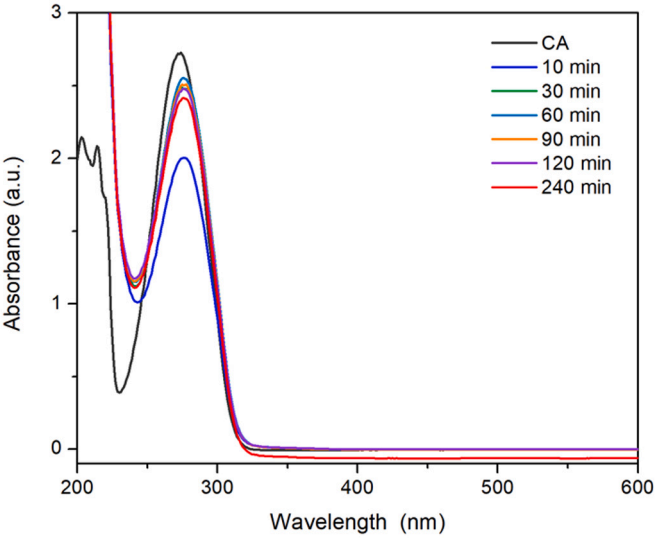

Fig. 8. UV–Vis spectrum: CA degradation with PS and Fe_2Mn_2.

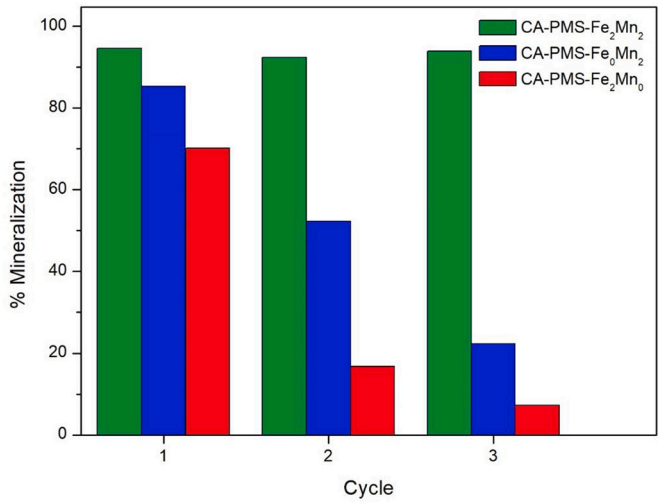

Fig. 9. Percentage of mineralization of CA with PMS and the catalyst series.

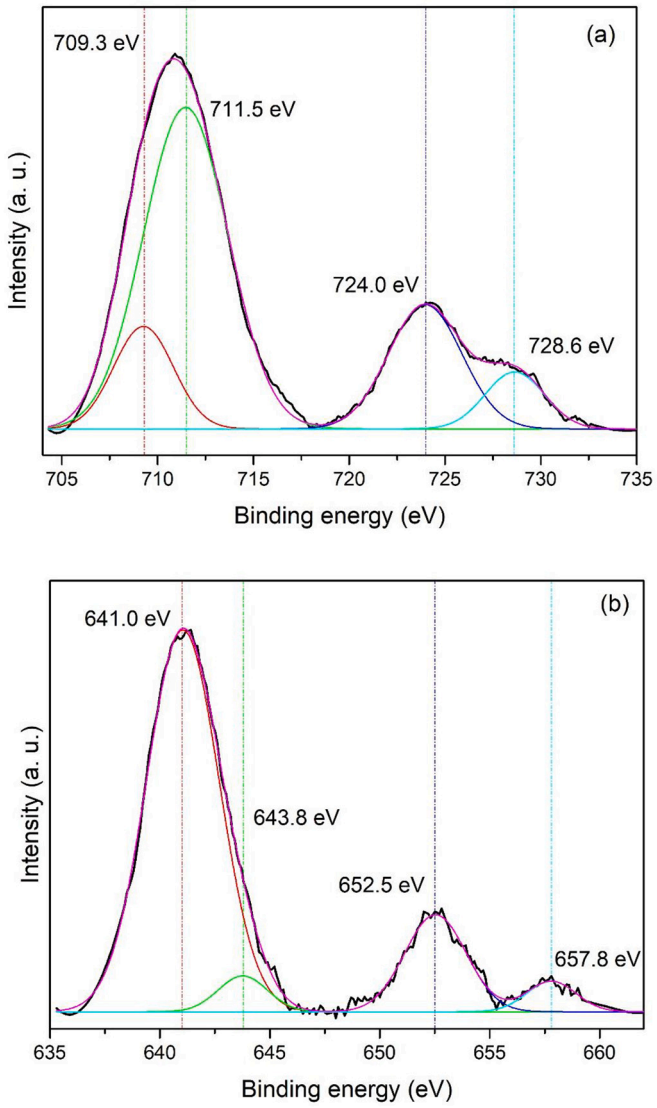

Fig. 10. XPS spectra of used Fe_2Mn_2. a) Fe 2p, b) Mn 2p.

c,d) and used Fe_2Mn_2 catalyst (Fig. 10).

After the catalytic reaction, the deconvoluted Fe 2p3/2 spectrum showed a change in the relative intensities of peaks attributable to Fe(II) and Fe(III), which could be attributed to a major transformation from Fe (II) to Fe(III). In the case of Mn, the Mn 2p 3/2 signals displayed a main peak at 641.0 eV, attributable to Mn(III) species, with a clear decrease in the intensity of those attributable to Mn(II) and Mn(IV). Thus, the slightly shift of values and the change in the relative intensities of the metal signals after the reaction with PMS and CA could be indicative of the participation of Fe(II)/Fe(III) and Mn(II)/Mn(III)/Mn(IV) redox cycles in the oxidant activation process. Moreover, the existence of surface trivalent Mn after the reaction would justify its high catalytic stability after several cycles of use in reaction, since oxidic Mn(III) species were found to be the most efficient for PMS activation, compared with Mn(II) and Mn(IV) oxides [43].

3.3.1. *Possible activation mechanism*

In recent years, several works have been published related to the synergistic effect in bimetallic catalysts, in particular, for catalysts based on Fe and Mn. Chen et al. [44] prepared a Fe—Mn catalyst supported on biochar and used it in the degradation of the acid red 88 dye employing PS as an oxidizing agent. With the same oxidant, Dong et al. [18] evaluated the degradation of bisphenol A with mixed oxides such as Fe_3O_4-α-MnO_2. In turn, Hao et al. [19] successfully degraded the azo dye Orange G with PS using catalysts based on biochar modified with Fe and Mn oxides. In these three cases, the XPS spectroscopy of the catalysts revealed the existence of Fe(II) and Fe(III) species, as well as Mn(II), in coincidence with the metallic species present in the materials reported in this article.

The mechanism proposed by these authors could apply to our PS activation reaction:

$$Fe(III) + Mn(II) \rightarrow Fe(II) + Mn(III) \quad (3)$$

$$Fe(II) + S_2O_8^{2-} \rightarrow Fe(III) + SO_4^{\bullet -} + SO_4^{2-} \quad (4)$$

$$Mn(II) + S_2O_8^{2-} \rightarrow Mn\ (III) + SO_4^{\bullet -} + SO_4^{2-} \quad (5)$$

$$Mn(III) + S_2O_8^{2-} \rightarrow Mn(IV) + SO_4^{\bullet -} + SO_4^{2-} \quad (6)$$

$$Fe(III) + S_2O_8^{2-} \rightarrow Fe(II) + S_2O_8^{\bullet -}\ (Eq.7)$$

$$Mn(IV) + S_2O_8^{2-} \rightarrow Mn(III) + S_2O_8^{\bullet -} \quad (8)$$

$$SO_4^{\bullet -} + H_2O \rightarrow SO_4^{2-} + OH\bullet + H^+ \quad (9)$$

Initially, the PS is activated by the action of Fe(II) and Mn(II) to generate the radicals $SO_4^{\bullet -}$, and oxidized Mn(III) species (eq. 4) could contribute to the generation of new radicals. The species Fe (III) and Mn (IV) are produced simultaneously through electronic transfer. Subsequently, the Fe and Mn species with higher oxidation states would be converted back to Fe (II) and Mn (III) via PS. All these reactions constitute a Fe/Mn transformation cycle. At the same time, some of the $SO_4^{\bullet -}$ radicals could react with water to generate $OH^{\bullet}$ radicals.

In the case of PMS, a large number of results were reported regarding the use of Fe—Mn bimetallic catalysts. To cite a few examples, Pang et al. [45] proposed a mechanism for the oxidative degradation of p-nitrophenol with this oxidant assisted by microwave and catalysed by $MnFe_2O_4$. Huang et al. [36] analyzed the degradation of bisphenol A using Mn—Fe nanospheres as a catalyst. Also, Yang et al. used ferromanganese oxides with different Fe / Mn ratios in the oxidative degradation of tetracycline with PMS [1]. According to the analysis of the results obtained by XPS for our system and based on what has been reported by different authors, the following activation mechanism can be proposed:

$$Fe(III) + Mn(II) \rightarrow Fe(II) + Mn(III) \quad (10)$$

$$Mn\ (II) + HSO_5^- \rightarrow SO_4^{\bullet -} + Mn\ (III) + OH^- \quad (11)$$

$$Fe\ (III) + HSO_5^- \rightarrow SO_5^{\bullet -} + Fe\ (II) + H^+ \quad (12)$$

$$Fe\ (II) + HSO_5^- \rightarrow SO_4^{\bullet -} + Fe\ (III) + OH^- \quad (13)$$

$$Mn\ (III) + HSO_5^- \rightarrow SO_4^{\bullet -} + Mn\ (IV) + OH^- \quad (14)$$

$$Mn\ (IV) + HSO_5^- \rightarrow SO_5^{\bullet -} + Mn\ (III) + H^+ \quad (15)$$

$$Mn\ (III) + HSO_5^- \rightarrow SO_4^{\bullet -} + Mn\ (II) + H^+ \quad (16)$$

$$2SO_5^{\bullet -} \rightarrow 2SO_4^{\bullet -} + O_2 \quad (17)$$

$$SO_4^{\bullet -} + H_2O \rightarrow SO_4^{2-} + OH\bullet + H^+ \quad (18)$$

On the catalyst surface, the reduced Fe and Mn species activate PMS generating $SO_4^{\bullet -}$ radicals, while the highest valence states of these metals are reduced by HSO_5^- to complete the redox cycle. The $SO_5^{\bullet -}$ radicals can react with each other to give the $SO_4^{\bullet -}$ radical a more active species for oxidation. As in the case of PS, the $SO_4^{\bullet -}$ radical can react with water to generate $OH^\bullet$ radicals.

The synergy between Fe and Mn in the activation of oxidants is an area that has not been completely explored and from which many alternatives to explain the mechanism arise. In agreement with that reported by Pang et al. [45], in this work a high degree of phenolic compounds degradation was achieved using the Mn/Fe combination, suggesting that the effect between the metals exists even when Fe(II) is absent, playing Fe(III) species a key role in synergism with Mn, probably due to the electrons transfer among multiple oxidation states of Fe- Mn, thus enhancing the generation of reactive oxygen species.

4. Conclusion

Mono and bimetallic Fe—Mn catalysts supported on Z were synthesized and characterized. These catalysts were found to be stable and active in the degradation by AOP of potentially contaminating compounds that may be present in OMW. The Fe_2Mn_2 catalyst exhibited the best performance in up to 3 cycles of use, with levels of mineralization >90%. This efficiency is a product of both the metal content and the synergistic effect between Mn and Fe. The electron transfer between the Fe—Mn species on the support enables the generation of radicals and the regeneration of the catalyst active sites. This transfer is thermodynamically feasible and is an example of the synergy between both metals, since the change in the oxidation states of Fe and Mn allows the generation of a major number of active species for the degradation of the pollutants. The degradation of pollutants by $SO_4^{\bullet -}$ radicals, electrophilic species, is influenced by their chemical structure and the presence of functional groups.

CRediT authorship contribution statement

Camila M. Loffredo: Conceptualization, Methodology, Validation, Investigation, Visualization, Writing - original draft. **Mariana Dennehy:** Conceptualization, Methodology, Validation, Investigation, Visualization, Resources, Supervision, Project administration, Funding acquisition, Writing - review & editing. **Mariana Alvarez:** Conceptualization, Methodology, Validation, Investigation, Visualization, Resources, Supervision, Project administration, Funding acquisition, Writing - review & editing.

Declaration of Competing Interest

The authors declare the following financial interests/personal relationships which may be considered as potential competing interests: Mariana Alvarez reports financial support was provided by Secretaría de Políticas Universitarias.

Data availability

Data will be made available on request.

Acknowledgments

C.M.L. is a fellow of CONICET. M.A. is a CONICET researcher. This work was funded by SGCyT-UNS 24/Q096, PICTO COVIAR 2017–0112 and Agregando Valor VT42- UNS11738 research grants.

Appendix A. Supplementary data

Supplementary data to this article can be found online at https://doi.org/10.1016/j.catcom.2022.106578.

References

[1] Q. Yang, X. Yang, Y. Yan, et al., Heterogeneous activation of peroxymonosulfate by different ferromanganese oxides for tetracycline degradation: structure dependence and catalytic mechanism, Chem. Eng. J. 348 (2018) 263–270, https://doi.org/10.1016/j.cej.2018.04.206.
[2] W.W. Anku, M.A. Mamo, P.P. Govender, Phenolic compounds in water: sources, reactivity, toxicity and treatment methods, in: Phenolic Compounds - Natural Sources, Importance and Applications, InTech, 2017, https://doi.org/10.5772/66927.
[3] G. Zhao, J. Zou, X. Chen, et al., Iron-based catalysts for persulfate-based advanced oxidation process: microstructure, property and tailoring, Chem. Eng. J. 421 (P2) (2021), 127845, https://doi.org/10.1016/j.cej.2020.127845.
[4] A. Cassano, C. Conidi, C.M. Galanakis, R. Castro-Muñoz, Recovery of polyphenols from olive mill wastewaters by membrane operations, in: Membrane Technologies for Biorefining, Elsevier, 2016, pp. 163–187, https://doi.org/10.1016/B978-0-08-100451-7.00007-4.
[5] W. Yakhlef, R. Arhab, C. Romero, M. Brenes, A. de Castro, E. Medina, Phenolic composition and antimicrobial activity of Algerian olive products and by-products, Lwt. 93 (2018) 323–328, https://doi.org/10.1016/j.lwt.2018.03.044.
[6] C. Belaid, M. Khadraoui, S. Mseddi, M. Kallel, B. Elleuch, J.F. Fauvarque, Electrochemical treatment of olive mill wastewater: treatment extent and effluent phenolic compounds monitoring using some uncommon analytical tools, J. Environ. Sci. (China) 25 (1) (2013) 220–230, https://doi.org/10.1016/S1001-0742(12)60037-0.
[7] A.A. Deeb, M.K. Fayyad, M.A. Alawi, Separation of polyphenols from Jordanian olive oil mill wastewater, Chromatogr. Res. Int. 2012 (2012) 1–8, https://doi.org/10.1155/2012/812127.
[8] H. Baati, A. Gargouri, E. Ammar, R. Jarboui, F. Fetoui, N. Gharsallah, Yeast performance in wastewater treatment: case study of Rhodotorula mucilaginosa, Environ. Technol. 33 (8) (2012) 951–960, https://doi.org/10.1080/09593330.2011.603753.
[9] T.R. Monisha, M. Ismailsab, R. Masarbo, A.S. Nayak, T.B. Karegoudar, Degradation of cinnamic acid by a newly isolated bacterium Stenotrophomonas sp. TRMK2, 3 Biotech 8 (8) (2018) 368, https://doi.org/10.1007/s13205-018-1390-0.
[10] N. Flores, A. Thiam, R.M. Rodríguez, et al., Electrochemical destruction of trans-cinnamic acid by advanced oxidation processes: kinetics, mineralization, and degradation route, Environ. Sci. Pollut. Res. 24 (7) (2017) 6071–6082, https://doi.org/10.1007/s11356-015-6035-9.
[11] F. Ghanbari, M. Moradi, Application of peroxymonosulfate and its activation methods for degradation of environmental organic pollutants: review, Chem. Eng. J. 310 (2017) 41–62, https://doi.org/10.1016/j.cej.2016.10.064.
[12] X. Xia, F. Zhu, J. Li, et al., A review study on sulfate-radical-based advanced oxidation processes for domestic/industrial wastewater treatment: degradation, efficiency, and mechanism, Front. Chem. (2020) 8, https://doi.org/10.3389/fchem.2020.592056.
[13] Oh.W. Da, Z. Dong, T.T. Lim, Generation of sulfate radical through heterogeneous catalysis for organic contaminants removal: current development, challenges and prospects, Appl. Catal. B Environ. 194 (2016) 169–201, https://doi.org/10.1016/j.apcatb.2016.04.003.
[14] Y. Chen, Y. Liu, Y. Li, et al., Synthesis, application and mechanisms of ferro-manganese binary oxide in water remediation: a review, Chem. Eng. J. 388 (2020), 124313, https://doi.org/10.1016/j.cej.2020.124313.
[15] P. Duan, T. Ma, Y. Yue, et al., Fe/Mn nanoparticles encapsulated in nitrogen-doped carbon nanotubes as a peroxymonosulfate activator for acetamiprid degradation, Environ. Sci. Nano. 6 (6) (2019) 1799–1811.
[16] S. Yan, X. Zhang, Y. Shi, H. Zhang, Natural Fe-bearing of, manganese ore facilitating bioelectro-activation peroxymonosulfate for bisphenol A oxidation, Chem. Eng. J. 354 (2018) 1120–1131.
[17] G.-X. Huang, C.-Y. Wang, C.-W. Yang, P.-C. Guo, H.-Q. Yu, Degradation of bisphenol a by peroxymonosulfate catalytically activated with $Mn_{1.8}Fe_{1.2}O_4$ nanospheres: synergism between Mn and Fe, Environ. Sci. Technol. 51 (21) (2017) 12611–12618, https://doi.org/10.1021/acs.est.7b03007.

[18] Z. Dong, Q. Zhang, B.Y. Chen, J. Hong, Oxidation of Bisphenol a by Persulfate Via Fe3O4-A-MnO2 Nanoflower-Like Catalyst: Mechanism and Efficiency vol. 357, Elsevier B.V, 2019, https://doi.org/10.1016/j.cej.2018.09.179.
[19] H. Hao, Q. Zhang, Y. Qiu, et al., Insight into the degradation of Orange G by persulfate activated with biochar modified by iron and manganese oxides: Synergism between Fe and Mn, J. Water Process Eng. 37 (June) (2020), https://doi.org/10.1016/j.jwpe.2020.101470.
[20] X. Zhou, C. Luo, M. Luo, et al., Understanding the synergetic effect from foreign metals in bimetallic oxides for PMS activation: a common strategy to increase the stoichiometric efficiency of oxidants, Chem. Eng. J. 2020 (381) (June 2019), 122587, https://doi.org/10.1016/j.cej.2019.122587.
[21] N. Scotti, F. Bossola, F. Zaccheria, N. Ravasio, Copper–zirconia catalysts: powerful multifunctional catalytic tools to approach sustainable processes, Catalysts. 10 (2) (2020) 168, https://doi.org/10.3390/catal10020168.
[22] A.G. Sato, D.P. Volanti, D.M. Meira, S. Damyanova, E. Longo, J.M.C. Bueno, Effect of the ZrO_2 phase on the structure and behavior of supported Cu catalysts for ethanol conversion, J. Catal. 307 (2013) 1–17, https://doi.org/10.1016/j.jcat.2013.06.022.
[23] M.H. Zare, A. Mehrabani-Zeinabad, Photocatalytic activity of $ZrO_2/TiO_2/Fe_3O_4$ ternary nanocomposite for the degradation of naproxen: characterization and optimization using response surface methodology, Sci. Rep. 12 (1) (2022), https://doi.org/10.1038/s41598-022-14676-y.
[24] R.M.A. Iqbal, T. Akhtar, E. Sitara, et al., Development of $Ag_{0.04}ZrO_2$/rGO heterojunction, as an efficient visible light photocatalyst for degradation of methyl orange, Sci. Rep. 12 (1) (2022) 1–12, https://doi.org/10.1038/s41598-022-16673-7.
[25] S.P. Keerthana, R. Yuvakkumar, P. Senthil Kumar, G. Ravi, D. Velauthapillai, Nd doped ZrO_2 photocatalyst for organic pollutants degradation in wastewater, Environ. Technol. Innov. 28 (2022), 102851, https://doi.org/10.1016/j.eti.2022.102851.
[26] P. Gao, Y. Song, M. Hao, A. Zhu, H. Yang, S. Yang, An effective and magnetic Fe_2O_3-ZrO_2 catalyst for phenol degradation under neutral pH in the heterogeneous Fenton-like reaction, Sep. Purif. Technol. 201 (February) (2018) 238–243, https://doi.org/10.1016/j.seppur.2018.03.017.
[27] P. Sakthisharmila, N. Sivakumar, J. Mathupriya, Synthesis, characterization of Mn, Fe doped ZrO_2 composites and its applications on photocatalytic and solar catalytic studies, Mater. Today Proc. (June 2021), https://doi.org/10.1016/j.matpr.2021.05.461.
[28] García EA, Rueda EH, Rouco AJ., Sulfated zirconia catalysts promoted with Fe and Mn: Mn effect in the Fe dispersion, Appl. Catal. A Gen. 210 (1–2) (2001) 363–370, https://doi.org/10.1016/S0926-860X(00)00827-9.
[29] García E, Volpe MA, Ferreira ML, Rueda E., A discussion of a mechanism for isomerization of n-butane on sulfated zirconia, J. Mol. Catal. A Chem. 201 (1–2) (2003) 263–281, https://doi.org/10.1016/S1381-1169(03)00123-7.
[30] S. Wacławek, K. Grübel, M. Černík, Simple spectrophotometric determination of monopersulfate, Spectrochim. Acta Part A Mol. Biomol. Spectrosc. 149 (2015) 928–933, https://doi.org/10.1016/j.saa.2015.05.029.
[31] C. Liang, C.-F. Huang, N. Mohanty, R.M. Kurakalva, A rapid spectrophotometric determination of persulfate anion in ISCO, Chemosphere. 73 (9) (2008) 1540–1543, https://doi.org/10.1016/j.chemosphere.2008.08.043.
[32] A.S. Diez, S. Schlichter, V. Tomanech, E.V.P. Miner, M. Alvarez, M. Dennehy, Spinel manganites synthesized by combustion method: structural characterization and catalytic activity in the oxidative degradation of organic pollutants, J. Environ. Chem. Eng. 5 (4) (2017), https://doi.org/10.1016/j.jece.2017.07.013.
[33] D. Gusain, P.K. Singh, Y.C. Sharma, Kinetic and equilibrium modelling of adsorption of cadmium on nano crystalline zirconia using response surface methodology, Environ. Nanotechnol. Monit Manag. 6 (2016) 99–107, https://doi.org/10.1016/j.enmm.2016.07.002.
[34] G. Balakrishnan, P. Kuppusami, S. Murugesan, E. Mohandas, D. Sastikumar, High temperature x-ray diffraction studies of zirconia thin films prepared by reactive pulsed laser deposition, Cryst. Res. Technol. 47 (4) (2012) 415–422, https://doi.org/10.1002/crat.201100229.
[35] C.R. Brundle, T.J. Chuang, K. Wandelt, Core and valence level photoemission studies of iron oxide surfaces and the oxidation of iron, Surf. Sci. 68 (C) (1977) 459–468, https://doi.org/10.1016/0039-6028(77)90239-4.
[36] G.X. Huang, C.Y. Wang, C.W. Yang, P.C. Guo, H.Q. Yu, Degradation of bisphenol a by peroxymonosulfate catalytically activated with Mn1.8Fe1.2O4 Nanospheres: synergism between Mn and Fe, Environ. Sci. Technol. 51 (21) (2017) 12611–12618, https://doi.org/10.1021/acs.est.7b03007.
[37] Z.P. Chen, J. Xing, H.B. Jiang, H.G. Yang, Visible-light-responsive photocatalyst for hydrogen evolution, Chem. - A Eur. J. 19 (2013) 4123–4127.
[38] Q. Tang, L. Jiang, J. Liu, S. Wang, G. Sun, Effect of Surface Manganese Valence of Manganese Oxides on the Activity of the Oxygen Reduction Reaction in Alkaline Media, 2014.
[39] Oh.W. Da, Z. Dong, T.T. Lim, Generation of sulfate radical through heterogeneous catalysis for organic contaminants removal: current development, challenges and prospects, Appl. Catal. B Environ. 194 (2016) 169–201, https://doi.org/10.1016/j.apcatb.2016.04.003.
[40] F. Mijangos, F. Varona, N. Villota, Changes in solution color during phenol oxidation by fenton reagent, Environ. Sci. Technol. 40 (17) (2006) 5538–5543, https://doi.org/10.1021/es060866q.
[41] Y.-T. Lin, C. Liang, J.-H. Chen, Feasibility study of ultraviolet activated persulfate oxidation of phenol, Chemosphere. 82 (8) (2011) 1168–1172, https://doi.org/10.1016/j.chemosphere.2010.12.027.
[42] H. Lin, S. Li, B. Deng, et al., Degradation of bisphenol a by activating peroxymonosulfate with Mn0.6Zn0.4Fe2O4 fabricated from spent Zn-Mn alkaline batteries, Chem. Eng. J. 364 (2019) 541–551, https://doi.org/10.1016/j.cej.2019.01.189.
[43] E. Saputra, S. Muhammad, H. Sun, H.M. Ang, M.O. Tadé, S. Wang, Manganese oxides at different oxidation states for heterogeneous activation of peroxymonosulfate for phenol degradation in aqueous solutions, Appl. Catal. B Environ. 142-143 (2013) 729–735, https://doi.org/10.1016/j.apcatb.2013.06.004.
[44] L. Chen, X. Jiang, R. Xie, Y. Zhang, Y. Jin, W. Jiang, A novel porous biochar-supported Fe-Mn composite as a persulfate activator for the removal of acid red 88, Sep. Purif. Technol. 250 (June) (2020), 117232, https://doi.org/10.1016/j.seppur.2020.117232.
[45] Y. Pang, H. Lei, Degradation of p-nitrophenol through microwave-assisted heterogeneous activation of peroxymonosulfate by manganese ferrite, Chem. Eng. J. 287 (2016) 585–592, https://doi.org/10.1016/j.cej.2015.11.076.